International Journal of Geography and Geology
2022 Vol. 11, No. 2, pp. 43-61.
ISSN(e): 2305-7041
ISSN(p): 2306-9872
DOI: 10.18488/10.v11i2.3165

AIRBORNE MAGNETIC SURVEY AND REMOTE SENSING APPLIED TO STRUCTURAL STUDY IN VOHILAVA AREA MADAGASCAR

Razananirina Henri[1+]
Rakotondrazafy Raymond[2]

[1,2]*Antananarivo University, Madagascar.*
[1]*Email: henrirazananirina@mgc.mg*
[2]*Email: raymondrakoto@gmail.com*

(+ Corresponding author)

Article History
Received: 29 July 2022
Revised: 19 September 2022
Accepted: 3 October 2022
Published: 13 October 2022

Keywords
Magnetometry
Pull-apart basin
Remote sensing
Riedel shear
Strike-slip faults
Vohilava.

ABSTRACT

Mananjary district is known for its gold production. To better understand the gold mineralization distribution, a regional structural study was undertaken using airborne geophysics and remote sensing (RS). Magnetometry data, Landsat Operational Land Imager (OLI) 8 satellite-image and DEM (Digital Elevation Model) have been processed and interpreted. Signals associated with deep structures are weak and dominated by strong signals from surficial magnetic sources. To overcome this problem, local-phase based filters were used. A deep knowledge of each filter allows to use it separately or in combination with other filters. RS is a powerful tool for a regional study. Color composite technique and DEM analysis were helpful to bring out faults and structures. The combination of magnetometry and RS allows geologists to efficiently delineate prospective zones. The study has unveiled a dextral strike-slip fault (SSF) over 240km and associated faults, folds, flower structure and pull-apart basins within the Mananjary gold district. Moreover, the SSF structurally controlled the spatial distribution of Vohilava-Nosivolo and Maha groups. R Riedel shear faults appear as North North East – South South West faults. R' Riedel shear faults occur in the north of the study area with East North East -West South West orientation. Tectonic block rotation occurred between Ampasinambo and Soavina. P' shear faults striking West North West – East South East occur in Vohilava. Some folds are associated with the SSF as well. Vohilava positive flower structure which used to be a syncline and its antiform equivalent are SSF footprints. The latter was active since Mesoarchean.

Contribution/Originality: The study helps understand structural elements which might control gold mineralization in Mananjary District Madagascar. The discovery of Vohilava SSF makes the area permissive for associated gold deposit types.

1. INTRODUCTION

Mananjary gold District is known by its gold panning activities and production. Nonetheless, no detailed studies have been conducted to date in the area. The area was mapped at 1/100000 scale for the first time in 1960's by H. Besairie. Then a Soviet Mission carried out the study in 1980's to produce gold potential map scale 1/100000. And lastly, Madagascar Government project called "Programme de Gouvernance des Ressources Minerales" funded by the World Bank renewed the mapping at scale 1/100000 in 2000's. A synthesis of Madagascar geology scale 1/1 000 000 was performed by British Geological Survey (BGS)-United States Geological Survey (USGS) consortium in 2012. The lack of data undermines the effort to promote exploration and attract investment which is a sine qua non for a large deposit discovery.

The study has two-fold objective which is the identification of key structural elements controlling the gold mineralization and a better delineation of prospective zones not only for alluvial deposit types but also for low sulphide-gold quartz veins. Application of the latest findings in remote sensing and geophysics combined with the use the new geological concept of domain, group and suite in the geology of Madagascar may open avenue to a discovery of large-scale gold deposits in Vohilava area.

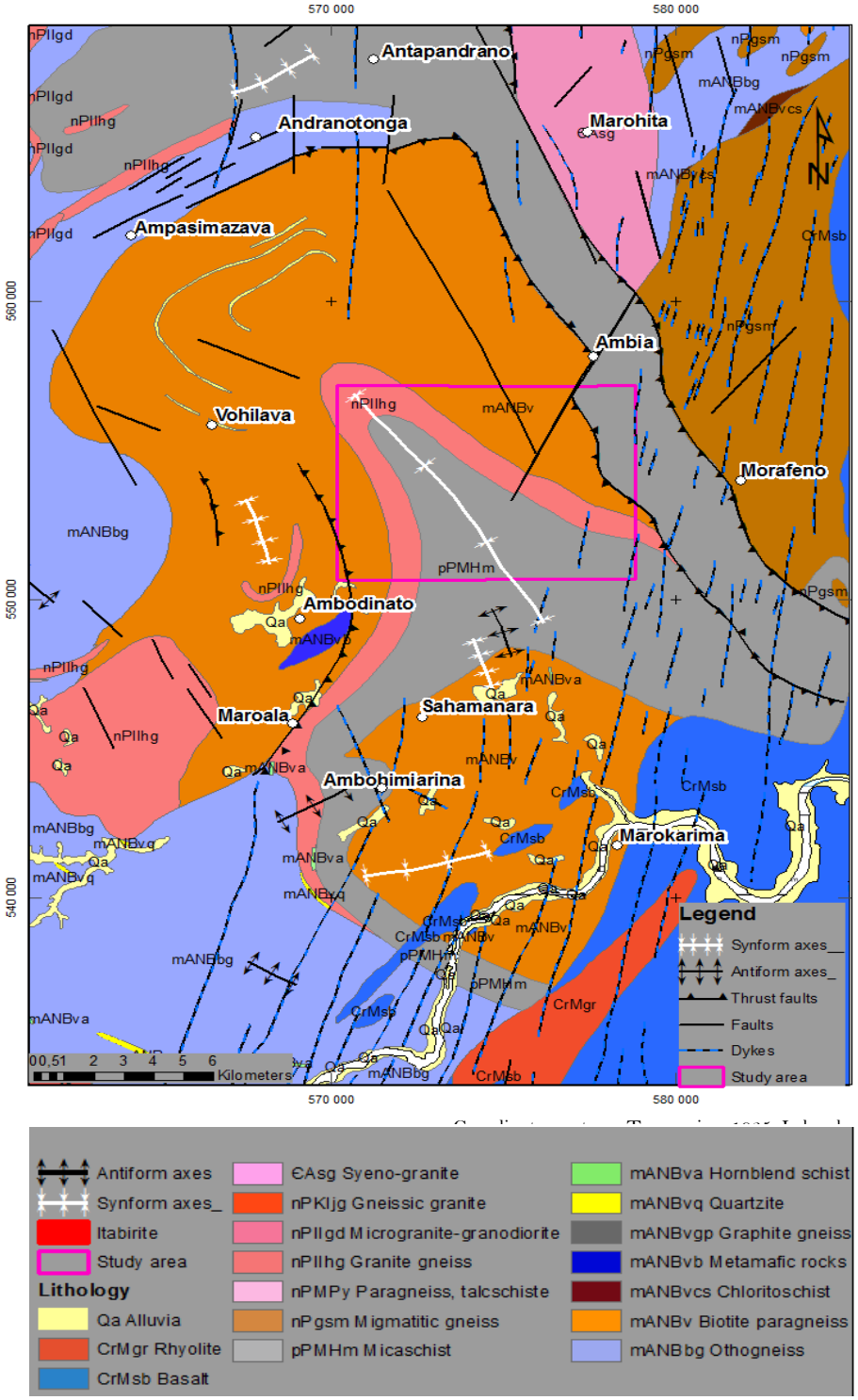

Figure 1. Geological map of Manakana area scale 1/100 000 (USGS-BGS, 2008b).

2. AREA OF STUDY

The area of study (AOS) is located at 30km distance North-West of Mananjary town in the South-East of Madagascar and covers 70 km². It is delimited by X=567 500m in the west, by X=577 500m in the east, by Y=552500m in the south and by Y=560000m the north in Laborde coordinate system Figure 1. The highest point is 380 meters while the lowest one is 20 meters. The hydrography of the AOS is characterized by Maha River which is flowing from the north-west to the south-east few kilometres to the north.

3. GEOLOGICAL SETTING

Geologically, Mananjary District is within the western part of the "Greater Dharwar" craton composed of Antongil/Masora and Antananarivo Domains. Like other shields in the world, Madagascar shield has three characteristics: -magmatic suite of tonalite, trondhjemite and granodioritic gneiss (TTG); -a volcano-sedimentary succession; - and syn- to post-tectonic granodiorite suite (Tucker, Peters, Roig, Théveniaut, & Delor, 2012). The AOS is contained within the Masora sub-Domain. It is composed of:

- Befody migmatitic orthogneiss belonging to the Nosy Boraha suite of Mesoarchean age (3.3-3.1Ga) and composed of quartzo-feldspathic gneiss with biotite sometimes with migmatitic hornblende, mainly granodioritic to tonalitic orthogneiss; It is the nucleus of the Madagascar Precambrian shield; Nd and Sr isotope ratios analysis indicates a juvenile origin of these formations from a depleted mantle and without any contribution of older crust.

- Vohilava-Nosivolo group which is bounded by Maha group in the east and Manampotsy group in the west. It is composed of two sub-groups namely Vohilava of Meso- Neoarchean and Nosivolo of Paleoproterozoic ages. It is composed of undifferentiated schist and mica gneiss with biotite, muscovite, garnet, kyanite, sillimanite and some minor banded iron formation with garnet and quartzo-feldspathic gneiss. The group is characterized by higher degree metamorphism comparatively with the surrounding Maha and Manampotsy groups. Its degree of metamorphism is indicated by the presence of kyanite, some sillimanite and alkaline feldspar assemblage. Vohilava sub-group includes as well layers and lenses of muscovite quartzite and fuschite.

- Maha group of turbiditic origin is Paleoproterozoic. It is composed of mica schist with quartzite, metapsammite, quartzo-feldspathic gneiss and graphitic rocks.
- Manampotsy group located in the far west outside the AOS is composed schist and quartzo-feldspathic gneiss containing several levels enriched in graphite; the group contains piles and lenses of mafic and ultramafic rocks, which have undergone the same tectonic and metamorphic events as the hosting paragneiss.
- A very wide Neoproterozoic migmatitic gneiss and nebulitic granite occurrence adjoins the eastern boundary of the study area;
- Cambrian syeno-granite Ambalavao suite covering more than 45km² can be observed 4km to the north;
- Upper-Cretaceous microgabbro and basaltic dykes (87.4Ma) oriented N010° to N016°;
- And Quaternary undifferentiated alluvium Figure 1.

A synform with N140° axis overlays the study area. En-échelon thrust faults parallel to the synform axis can be observed on both sides of the structure. Two faults oriented N030° and N155° intersect with each other at 4km distance SW of Ambia village.

4. METHODOLOGY

In this study, a combination of remote sensing and airborne magnetic survey was used. The regional character of the study and the relative low cost of the used method justify the choice.

4.1. Magnetometry and Data Processing

Airborne magnetometry data acquired on behalf of the Malagasy Government during the Programme de Gouvernance des Ressources Minerales in year 2000s are available and have been used.

Data have been processed using Geosoft Oasis Montaj. Measured total magnetic intensity (TMI) of the magnetic field was corrected using International Geomagnetic Reference Field (IGRF) to produce the magnetic anomaly field. The latter has 3 components T_x, T_y and T_z disposed in orthogonal coordinate system. T_x and T_y are in the horizontal plan, whereas T_z is the measured vertical component.

$$T^2=T_x^2+T_y^2+T_z^2$$

As T is dependent of the inclination of the magnetic field, the curve is asymmetric except at the poles. To avoid asymmetry of the curve and make interpretation easier, the IGRF corrected TMI is reduced to pole (RTP). Further processing is based on the RTP grid data. Different transformations have been made to produce more practical field for interpretation, decompose anomaly, amplify subtle anomalies and separate two closely spaced sources. The following step of the processing was to calculate the partial derivative of the 3 components of T.

$$\frac{\partial T}{\partial x}=\frac{T_{i+1}-T_{i-1}}{x_{i+1}-x_{i-1}};\qquad \frac{\partial T}{\partial y}=\frac{T_{i+1}-T_{i-1}}{y_{i+1}-y_{i-1}};\qquad \frac{\partial T}{\partial z}=\frac{T_{i+1}-T_{i-1}}{z_{i+1}-z_{i-1}}$$

Geometrical relationship between initial field T, 1st order VD, AS, THDR, TDR (TA), ETilt and ETHDR is shown below Figure 2. Some useful formulas are inserted into the diagram for practical purpose.

Total magnetic field derivatives are necessary when the geology is complex or details are required. The standard filter package can include the following:

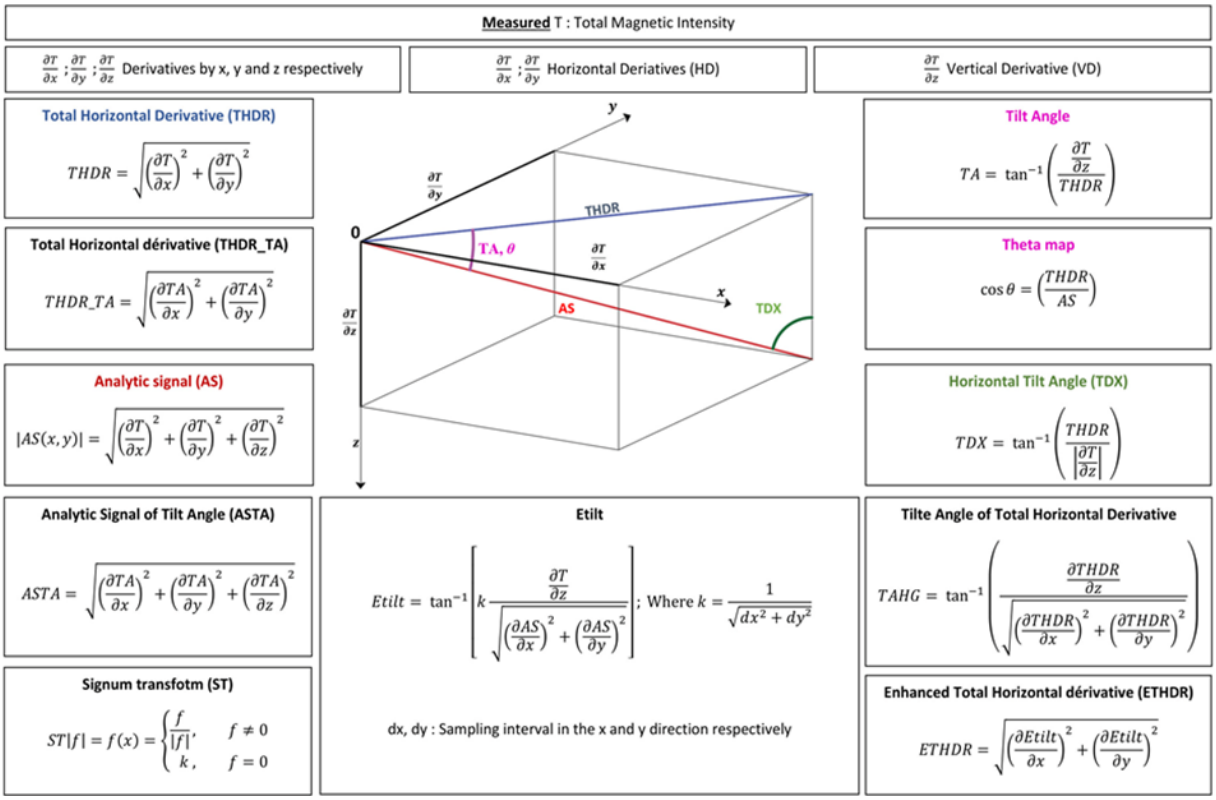

Figure 2. Definition of the geometrical relationships between first-order vertical derivative (VD), total horizontal derivative (THDR), analytic signal (AS), tilt angle (TA) or TDR, theta-map and horizontal tilt angle (TDX); Useful formulas inserted into the diagram.

Horizontal derivative (HD) or horizontal gradient enhances edges of magnetic source and is efficient when dealing with linear anomalies. The direction has to be perpendicular to the main structures or the targeted anomalies for a better result. As the curve is asymmetric, it is very practical to reduce the HD to pole in order to make the interpretation easier.

Vertical derivative (VD) or vertical gradient is used widely in magnetic data interpretation. The curve crosses the zero line approximately above the edge of the magnetic source and remains positive above it. It enhances the high

wavenumber component of the magnetic field, as a result the width of the anomaly is narrow and the source location is more accurate. It works well for near-surface geological features.

Total horizontal derivative (THDR) introduced by Cordel and Grauch in 1985 is an amplitude-based filter and uses 1st order derivatives of T.

$$\text{THDR} = \sqrt{\left(\frac{\partial T}{\partial x}\right)^2 + \left(\frac{\partial T}{\partial y}\right)^2};$$

It is not only less sensitive to the noise in the data but also robust in detection of shallow magnetic sources (Ismael, Menna, & Bülent, 2019). The curve shows high amplitude over the source edge. THDR provides high accuracy in the edge delineation.

Analytic signal amplitude (ASA) or total derivative is another amplitude-based filter.

$$|\text{ASA}| = \sqrt{\left(\frac{\partial T}{\partial x}\right)^2 + \left(\frac{\partial T}{\partial y}\right)^2 + \left(\frac{\partial T}{\partial z}\right)^2};$$

The curve is always positive and has the maximum value above the edge of the source. ASA anomaly shape is independent of magnetization direction of the 2D source. Thus, it allows to delineate the source geometry. The main disadvantages are the low spatial resolution which does not allow to separate two closely spaced sources and in case of more than one source is present, high amplitude signals from shallow sources dominate and obscure subtle ones.

Tilt derivative (TDR) suggested by Miller and Singh (1994) is the *Tilt angle (TA)* which is defined as the arctangent function of the ratio of 1st order vertical derivative to the total horizontal derivative.

$$\text{TDR} = \tan^{-1}\left(\frac{\left(\frac{\partial T}{\partial z}\right)}{\sqrt{\left(\frac{\partial T}{\partial x}\right)^2 + \left(\frac{\partial T}{\partial y}\right)^2}}\right)$$

As the curve of the function varies from $-\pi/2$ to $+\pi/2$, all signals including high amplitude ones are compressed within the said range. This way, weak signals are relatively enhanced with respect to high amplitude ones. Although it brings out weak signals, deep edges are blurred. Disadvantages are that TA enhances noise in the data and is relatively less sensitive to the source depth. As it was defined, it does not contain information on the strength of the geomagnetic field nor the susceptibility of the causative bodies. The tilt angle amplitudes depend strongly on magnetic field inclination (Shahverdi, Namaki, Montahaei, Mesbahi, & Basavand, 2017).

To compensate the disadvantage of the tilt angle, Fairhead, Green, Verduzco, and Mackenzie (2004) introduced the *total horizontal derivative of the tilt angle (HD_TDR)* or simply *(THDR_TA)*, which works *better* than TA does on deep source edges. HD_TDR is based on derivative of derivative; therefore, it is sensible to noise.

Enhanced Total Horizontal Derivative (ETHDR) was introduced by Arisoy and Dikmen (2013) as edge detector. It is defined as the total horizontal derivative of ETilt.

Using the same formula as for tilt angle, keeping $\frac{\partial T}{\partial z}$ as vertical component in the computation and replacing $\frac{\partial T}{\partial x}$ and $\frac{\partial T}{\partial y}$ by $\frac{\partial AS}{\partial x}$ and $\frac{\partial AS}{\partial y}$ respectively, a new angle called enhanced tilt angle (ETilt) is obtained.

$$\text{ETilt} = \tan^{-1}\left(\frac{\left(\frac{\partial T}{\partial z}\right)}{\sqrt{\left(\frac{\partial AS}{\partial x}\right)^2 + \left(\frac{\partial AS}{\partial y}\right)^2}}\right); \text{ with } \quad \frac{\partial AS}{\partial x} = \frac{AS_{i+1} - AS_{i-1}}{X_{i+1} - X_{i-1}}; \quad \frac{\partial AS}{\partial y} = \frac{AS_{i+1} - AS_{i-1}}{Y_{i+1} - Y_{i-1}}$$

$$\text{ETHDR} = \sqrt{\left(\frac{\partial ETilt}{\partial x}\right)^2 + \left(\frac{\partial ETilt}{\partial y}\right)^2};$$

ETHDR is a powerful edge detector filter. It is expressed in radian/meter. The filter produces more detailed results for deeper magnetized structures and gives sharp responses over edges (Arisoy & Dikmen, 2013). It performs

well on both shallow and deep sources and offers high spatial resolution. The filter is efficient in separating two closely spaced deep bodies. As the filter is based on derivative of derivative, it is sensible to noise.

Horizontal tilt angle (TDX) suggested b Cooper and Cowan (2006) which is defined as arctangent of the ratio of total horizontal derivative to the absolute value of the vertical derivative. When crossing the source edge, the value of vertical derivative is zero, therefore TDX tends towards its maximal value which is $+\boldsymbol{\pi}/2$. Although TDX works well for shallow and deep sources, it still has a weakness which is the tendency to show a wider anomaly than the causative body when more than one source is present.

$$\mathrm{TDX} = \tan^{-1}\left(\frac{(THDR)}{|\frac{\partial T}{\partial z}|}\right)$$

Theta map [cos (θ)] introduced by Williams and Fairhead (2006) where the total horizontal derivative is normalized by the amplitude of the analytic signal. Since the function varies from 0 to +1, when crossing the edge $\frac{\partial T}{\partial z} \rightarrow 0$, thus cos (θ) →1. At the edges of causative body, amplitude of the signal is the same regardless of the source depth (Cooper & Cowan, 2006). As the function includes AS, it works well on all causative bodies regardless of the source orientation.

$$\cos(\theta) = \frac{THDR}{ASA};$$

Tilt Angle of Horizontal Gradient (TAHG) as defined by Ferreira, Souza, Bongiolo, and Castro (2013) is the arctangent of the normalized value of vertical derivative of total horizontal derivative by the total horizontal derivative of the total horizontal derivative.

$$\mathrm{TAHG} = \tan^{-1}\left(\frac{\left(\frac{\partial THDR}{\partial z}\right)}{\sqrt{\left(\frac{\partial THDR}{\partial x}\right)^2 + \left(\frac{\partial THDR}{\partial x}\right)^2}}\right)$$; where THDR is the total horizontal derivative.

The filtered value varies from $-\pi/2$ to $+\pi/2$. TAHG equalizes the signals obtained from shallow and deep sources. This method has two notable features: I- it produces maximum amplitudes over the edges of the sources, II- it gives suitable resolution and is less dependent on the structure depths. It performs well on both shallow and deep causative bodies. The deep source thickness defined by TAHG is more accurate than the one obtained using TDX (Ferreira et al., 2013). Furthermore, the TAHG method has better resolution in determining the boundaries of deeper sources than TDR method (Shahverdi et al., 2017). However, like the TDR, this method depends on the inclination of magnetic field.

Analytic signal of Tilt angle (ASTA) suggested by Ansari and Alamdar (2011) is a combination of two filters namely analytic signal and tilt angle. The curve has maximum value over the body edges and offers a better accuracy in edge detection than original filters separately (Ansari & Alamdar, 2011). It allows to detect signals from both shallow and deep causative bodies.

$$\mathrm{ASTA} = \sqrt{\left(\frac{\partial TA}{\partial x}\right)^2 + \left(\frac{\partial TA}{\partial y}\right)^2 + \left(\frac{\partial TA}{\partial z}\right)^2}$$; where TA is the tilt angle.

Signum transform (ST) suggested by Souza and Ferreira (2015) is a simple derivative-based method for qualitative and quantitative interpretation of magnetic anomalies from dyke-like structures. The method is based on the normalization the filtering function by its absolute value.

$$\mathrm{ST}\,|f| = f(x) = \begin{cases} \frac{f}{|f|}, & f \neq 0 \\ k, & f = 0 \end{cases}$$

Therefore, the filtered anomaly value will have only two values (-1 or +1). The causative source will have the value +1. It was suggested to use first-order vertical derivative of the magnetic anomaly, second-order vertical derivative or first-order vertical derivative minus total horizontal derivative as filtering function (Souza & Ferreira,

2015). Signum transform of second-order vertical derivative has given better results in this study. It is efficient in separating two closely spaced bodies leading to a superposition of anomalies.

Depending on the complexity of the geology, the geological task and the acquired data quality, different filters are applied to produce maps. When dataset contains high variation of amplitude, the output of derivative based filters is dominated by high amplitude anomalies which hide subtle signals. Then local phase filters are processed in order to bring out the latter. It can be the case when the magnetic susceptibility contrast between two formations is not enough to generate anomaly visible on RTP. Edge detector filters as TDR, TDX, HD-TDR, Theta map, ETHDR and signum transforms are produced to find details of structures. With the increasing derivative order, information details and noise are increasing as well.

4.2. Remote Sensing

The regional character of the study requires a quick and relatively cheap exploration method as remote sensing using satellite images. Landsat 8 and digital elevation model were available and downloaded free of charges for the study.

4.2.1. Landsat 8

Two Landsat images scene LC81580742014364LGN00 and LC81580752014364LGN00 were downloaded from https://earthexplorer.usgs.gov on 23/12/2014 and 05/01/2015 respectively to cover the AOS. A mosaic image was produced to cover the AOS. For further analysis, it was necessary that both 100meter resolution thermal infrared (TIR) bands and the panchromatic band 8 had the same spatial resolution as the visible and near infrared (VNIR) and short-wave infrared (SWIR) and have been resampled to 30 meters. It was a requisite for the combination of bands using TIR in color composite or ratio composite images. A 15meter panchromatic band 8 is used when a better spatial resolution (15 meters) is required.

Table 1. Matrix showing correlation between bands.

Correlation	OLI 1	OLI 2	OLI 3	OLI 4	OLI 5	OLI 6	OLI 7	OLI 8	TIR 1	TIR 2
OLI 1	1.000	0.950	0.116	0.161	-0.549	-0.400	-0.233	0.169	-0.025	-0.113
OLI 2	0.950	1.000	0.383	0.420	-0.375	-0.172	0.006	0.421	0.028	0.008
OLI 3	0.116	0.383	1.000	0.919	0.627	0.749	0.779	0.925	0.225	0.487
OLI 4	0.161	0.420	0.919	1.000	0.491	0.742	0.842	0.924	0.208	0.477
OLI 5	-0.549	-0.375	0.627	0.491	1.000	0.883	0.738	0.520	0.208	0.497
OLI 6	-0.400	-0.172	0.749	0.742	0.883	1.000	0.958	0.703	0.221	0.543
OLI 7	-0.233	0.006	0.779	0.842	0.738	0.958	1.000	0.770	0.215	0.524
OLI 8	0.169	0.421	0.925	0.924	0.520	0.703	0.770	1.000	0.213	0.465
TIR 1	-0.025	0.028	0.225	0.208	0.208	0.221	0.215	0.213	1.000	0.435
TIR 2	-0.113	0.008	0.487	0.477	0.497	0.543	0.524	0.465	0.435	1.000

Color composite technique was used to produce images for interpretation. Different bands can be combined to create colored images. As sensors record correlated information, it is judicious to combine the least correlated bands for better images. A statistics of data composing Landsat 8 bands excluding Band 9 (cirrus) has been computed Table 1. On the basis of the correlation matrix, the best composition is expected when Band 7, Band 3 and Band 2 are respectively assigned to Red (R), Green (G) and Blue (B) (RGB732) Figure 3a. It usually works when the humidity in the atmosphere is low. The fact that the AOS is located in a tropical region where climate is humid and vegetation is almost ubiquitous requires another approach. Among bands designed for water particle detection, OLI 3 and OLI 4 bands are comparatively less sensitive to humidity as they have relatively low reflectance from water. Regarding the vegetation, spectral analysis showed that OLI 4 band displays absorption of electromagnetic waves by biomass while the OLI 7 records a very low reflectance from biomass. The optimal and suitable color composite image for this region is then RGB743 which has given the clearest image for geological feature extraction Figure 3b.

Coordinate system: Tananarive 1925 Laborde Grid.

(a) (b)

Figure 3. OLI 2 band more sensitive to water particule in the atmosphere than OLI 3. Better image obtained from the colour composite RGB743 (b) than RGB732 (a). Note the blue color representing the humidity in the atmosphere on figure-3a.

4.2.2. Digital Elevation Model ASTGTM

The Terra Advanced Spaceborne Thermal Emission and Reflection Radiometer (ASTER) Global Digital Elevation Model (GDEM) Version 3 called ASTGTM provides a DEM of land areas on Earth at a spatial resolution of 1 arc second (approximately 30 meters horizontal posting at the equator). Four ASTGTM namely ASTGTMV003_S21E047, ASTGTMV003_S21E048, ASTGTMV003_S22E047 and ASTGTMV003_S22E048 from USGS have been downloaded and a mosaic was produced. DEM gives basic information about geological structures and topographical features.

Different analysis techniques of the DEM namely hillshade, shaded relief and gradient image have been applied for the detection of structures and faults.

5. RESULTS AND DISCUSSION

5.1. Results from Magnetometry

RTP filter has given significant results in the identification of faults Figure 4. Some details have been revealed by different local phase filters as directional horizontal derivatives and signum transform map.

5.2. Remote Sensed Data Analysis Results

The 30-meter resolution Landsat 8 OLI image helped identify shear zones, faults, new folds and ductile deformations indicating shear senses. An extensional horsetail splay was unveiled in the south of Mahanoro whereas a contractional one was discovered in Ampasimanjeva area in the south. ASTGTM analysis led to pull-apart basins identification in Soavina and Ankazotsifantatra and a graben in Befody. An explanation was found for the Vohilava structure which is a positive flower structure. The presence of normal faults in Andranotonga was materialized by a rapid change in altitude. A combined interpretation of Landsat image and ASTGTM led to the discovery of the Ambia structure which is the antiform equivalent of Vohilava synform. The structure is very fragmented and has experienced horizontal displacement resulting in four separated antiforms.

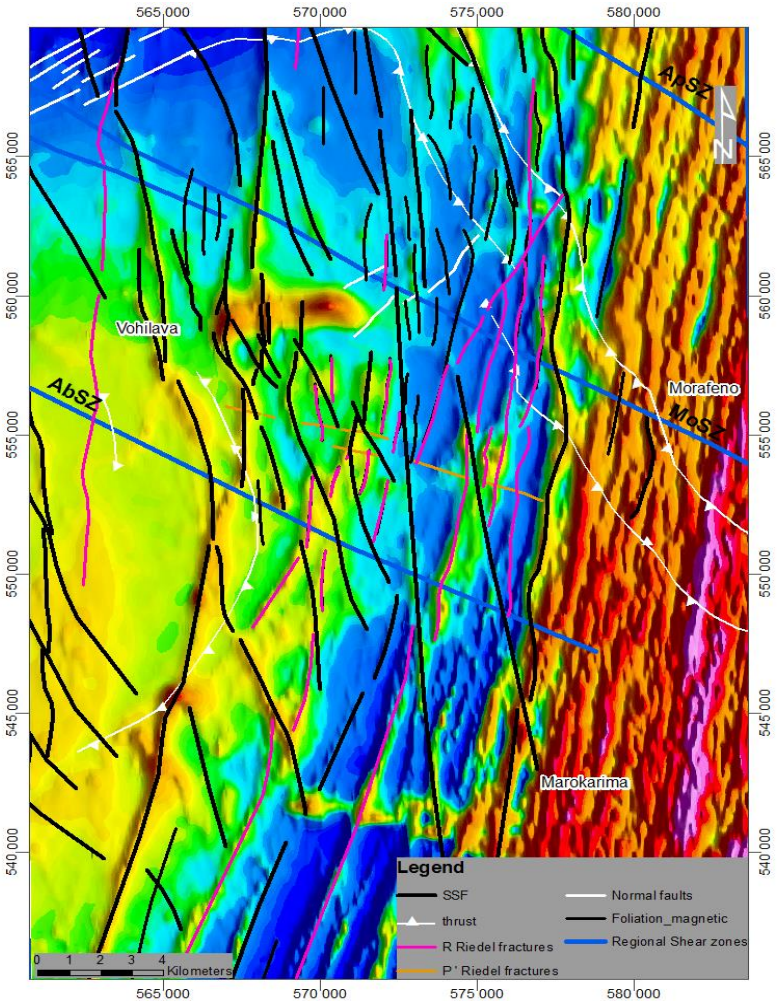

Coordinate system: Tananarive 1925 Laborde Grid

Figure 4. Total magnetic Intensity reduced to pole; Local anomalies are shown in the east of Vohilava. The east and the south-east of AOS are dominated by strong anomalies associated with dykes and volcanics. Curvy MSSF observed in the east.

5.3. Brittle and Ductile Deformations

Some faults fragments randomly distributed have been documented on geological maps scale 1/100 000 (USGS-BGS, 2008c). A group of thrust faults has been observed in Vohilava area. The association of thrust faults with SSF is well known in the world like Maine in the United States of America and San Andreas (Marvinney & Tucker, 1989). After lineament and structure extraction from magnetometry data and satellite image, and considering all existing faults in the map, a strike-slip fault which I call Vohilava strike-slip fault was unveiled between Ampasimanjeva village located in the northern part of the Fitovinany region and Menagisy village within Mahanoro District Antsinanana Regio Figure 5.

Where basalt or the microgabbro infill is present, the identification of the SSF fragments by magnetometric method does not present any difficulties. It has N018° direction from Irondro to Maroala then it goes NS up to Ampasinambo area before turning NE forming horsetail splay. Its strike length is above 240 kilometers. The study has shown that it has generated en-échelon thrust faults in Vohilava area, en-échelon normal faults with N057° azimuth in the east of Ampasimazava and in the north of Besaonjo villages and finally a flower structure which I call Vohilava structure, at tens of kilometers distance south east of vohilava village. The highest point within the structure taken from the digital elevation model is 380m. The eastern part in Irondro area is underlain by late cretaceous volcanic rocks which makes structure identification difficult. Structures in Vohilava area is in line with the dextral SSF model as defined by Sylvester and Smith (1976). A left-stepping of the Vohilava SSF is observed between

Marokarima and Marofototra. It is represented by a compressional bend measuring 65km in length and 35km in width and characterized by NNW-SSE fractures.

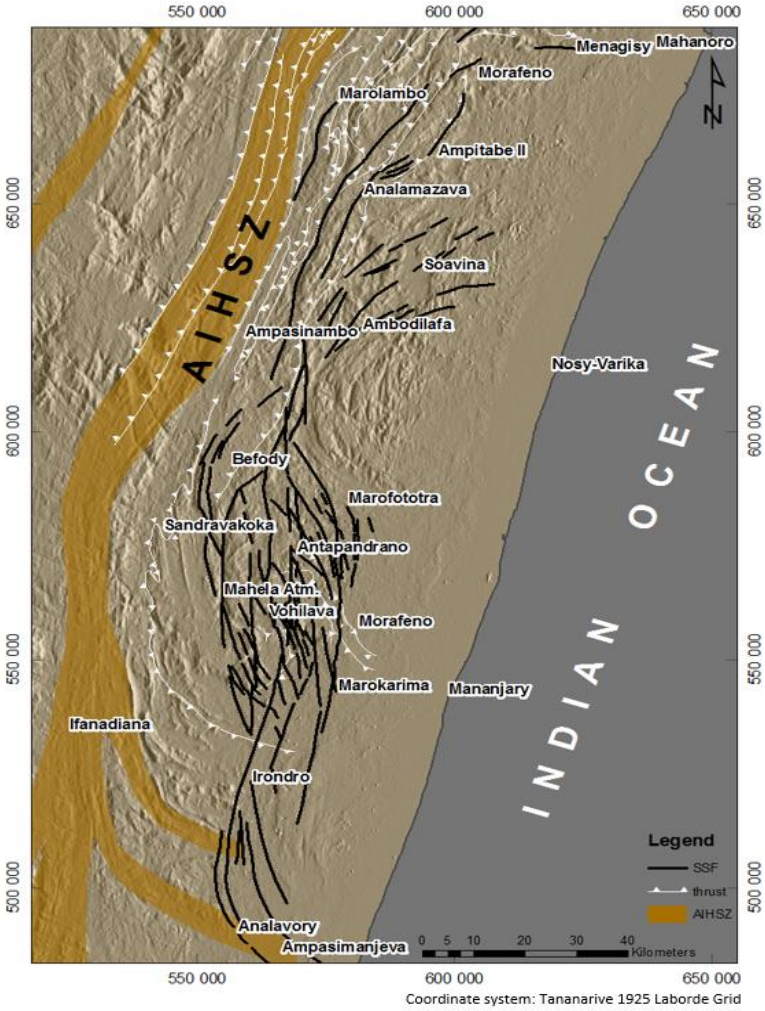

Figure 5. Tectonic map scale 1/750 000 showing AIHSZ, Vohilava SSF and associated thrust faults. Extensional horsetail splay in the north of Ampasinambo and contractional horsetail splay in Analavory and Ampasimanjeva in the south. Vohilava area representing a contractional duplex in a restraining bend.

R Riedel fractures oriented from N020° to N024° constitute the second group of faults in terms of occurrence in the area Figure 6. Three R shear fracture groups which I call Vohilava (Rv), Sahamanara (Rs) and Ambia (Ra) fractures. Rv and Rs are the most important in terms of length and strike over 40km and 38km respectively. They underwent brittle deformation in some places where the SSF or the regional SZ cross-cut the R fractures. In Marokarima area, horizontal displacements of the blocks resulting from master strike-slip fault (MSSF) activity are about 800m and 1600m in Ambohimiarina and Sahamanara respectively. A 12-kilometer dextral synthetic shear fracture oriented N028° is crossing Ambia and constitutes a Riedel fracture of the Vohilava SSF Figure 6. It is worth noting that two generations of R shear fractures are present in Ambia. The 1st one (Ra1) oriented N013° is associated with the N003° master SSF while the second generation (Ra2) with N028° azimuth is associated with the MSSF bend having N357° orientation. Ra2 cross-cut Ra1 and produced a right-lateral horizontal displacement of more than 400m distance. This displacement was documented on geological map N° R-52 scale 1/100 000 (USGS-BGS, 2008d). These shear fractures are also right-lateral as the main shear and represent opening for mineralizing fluids.

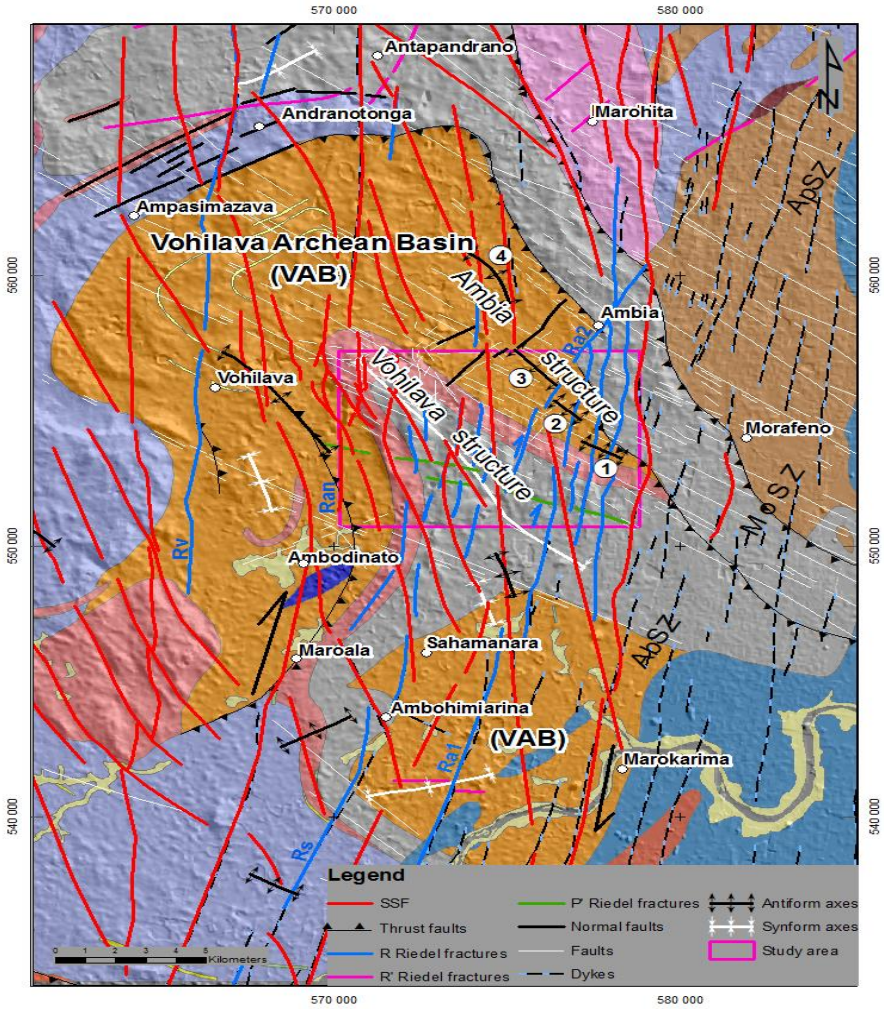

Figure 6. Geological map scale 1:100 000 modified from USGS-BGS (2008a). SSF crosscutting the Vohilava area. Ambia structure parallel to Vohilava structure. R shear, R' shear and P' shear faults developed respectively in the south, in the north and in the center. Thrust faults, normal faults, Riedel shear faults and folds orientation in line with a dextral SSF model.

R' shear fractures which are antithetic, sinistral in our case, were developed in Marofototra, Andranotonga and Antapandrano areas and represent openings as well. Directional HD map shows that the ENE-WSW sinistral R' in the north of Andranotonga is cross-cut by the N-S MSSF with 1km horizontal displacement between Andranotonga and Antapadrano. Between Antapandrano and Marofototra, R' faults group becomes dominant in terms of occurrence comparatively with R faults group. R' faults are oriented NE-SW and have strike length not exceeding 10km.

P' shear faults striking N105° to N110° with a very little horizontal displacement were identified in the SE of Vohilava village. Some N170° faults appearing as P' between Analamazava and Ampasinambo are not compressive faults. They were initially N150° R' fractures which underwent right-lateral block rotation of 20°. Initial faults are still observed between Analamazava and Soavina.

5.3.1. Pull-Apart Basins and Grabens

In the south of Mahanoro, the extension associated with the horsetail splay was very active during Proterozoic leading to the formation of another pull-apart basin which I call Ankazotsifantatra Proterozoic Basin (APB). The latter is overlain by Paleoproterozoic kyanite micaschist (pPMHn) Figure 7. Conversely, Vohilava sub-group occurrence does not go northward beyond the latitude of Marolambo and shows a very limited character or almost inexistent in the far north APB. During Paleoproterozoic, an NNW-SSE extension occurred in Andranotonga-Antapandrano area opening a N057° graben where Maha group protolith was deposited. N057° normal faults are dominant in this area. Contact between Mesoarchean migmatitic orthogneiss and Paleoproterozoic micaschist by

normal faults was mapped around Andranotonga. A 7km Imorona-Itsindro granitic dyke with N057° azimuth is good evidence of the extension. In Befody area, a 40 km elongated structure was mapped. The dextral SSF right stepping in Befody area created an extensional bend. The latter was characterized by subsidence, crustal thinning, significant basin sedimentation and important fluid flow (Cunningham & Mann, 2007). The structure was filled in with detritic materials resulting from the pre-existing migmatitic othogneiss erosion. Finally, two N-S pull-apart basins in the north of Ambodilafa and Soavina area host the Vohilava sub-group.

Ambia structure split in four parts:

1) East Manakana structure.

2) West Manakana structure.

3) Besaonjo structure.

4) West Ambia structure.

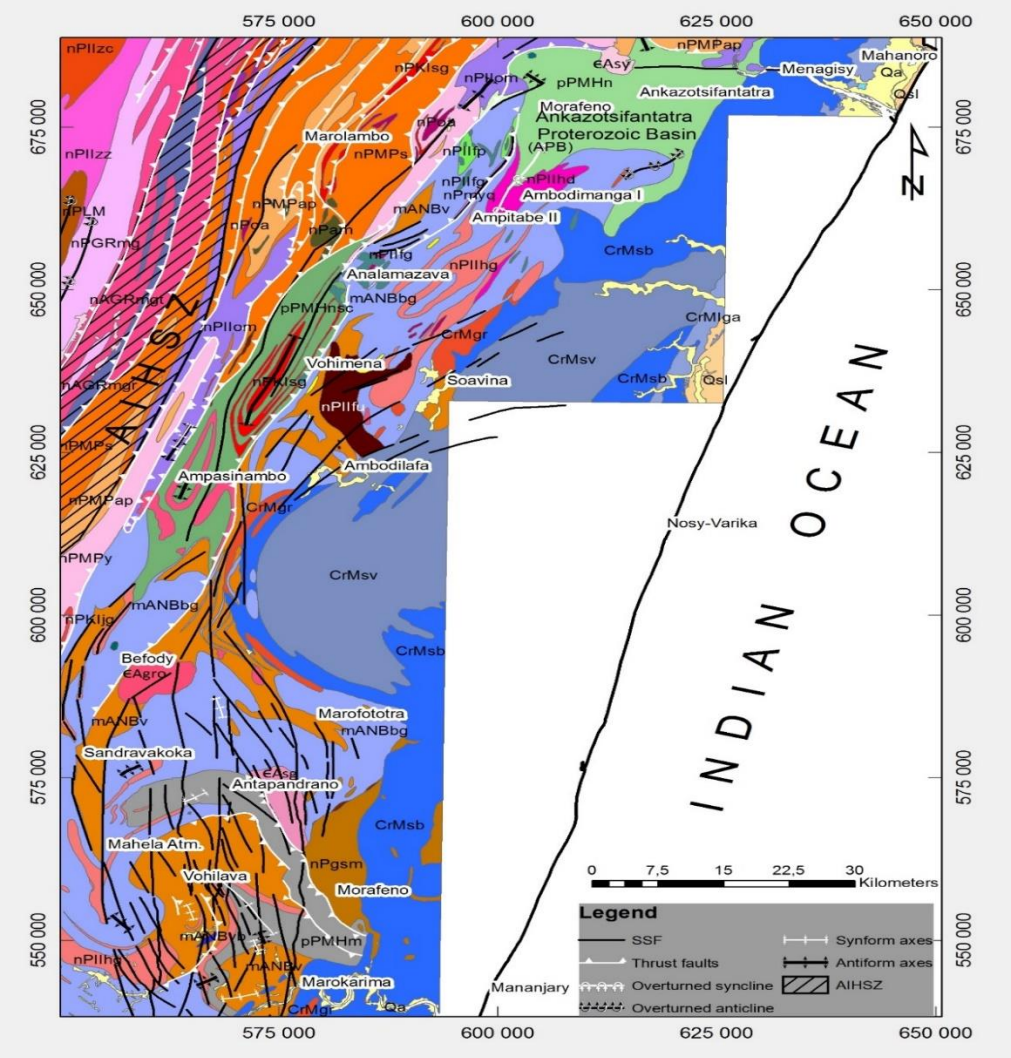

Figure 7. Geological map scale 1/500 000 modified from Tucker et al. (2012) showing the SSF control on the Vohilava-Nosivolo and Maha groups spatial distribution. Note the contractional duplex from Marokarima to Marofototra and the horsetail splay from Ampasinambo to Mahanoro.

5.3.2. Horsetail Splays

Single compressional and extensional bends forming horsetail splays were discovered at the SSF terminations. Extensional horsetail splay was identified from Ambodilafa to Mahanoro area. It was at the origin of the pull-apart basin in Soavina. Faults are curved and progressively turn north-east to east before disappearing. Note the occurrence of E-W faults in the south of Mahanoro. Landsat image interpretation revealed the presence of a compressional

horsetail splay between Irondro and Ampasimanjeva in the southern part of the AOS Figure 9. Compression resulted in reverse faults generation and blocks tilt. Evidence of the reverse faults occurrence within the structure was provided on a topographical profile EF extracted from DEM Figure 10. Looking at the fault F1, the hanging wall was tilted to the north-east and moved up relative to the foot wall. This reverse fault is evidence of shortening resulting from compressional forces. Fractures are progressively turning to the SE while moving southward to form imbricate fans. Faraony River follows the structure generated by the horsetail splay over 20km distance before reaching the Indian Ocean.

Figure 8 presents all formations within the area.

Figure 8. All formations within the area.

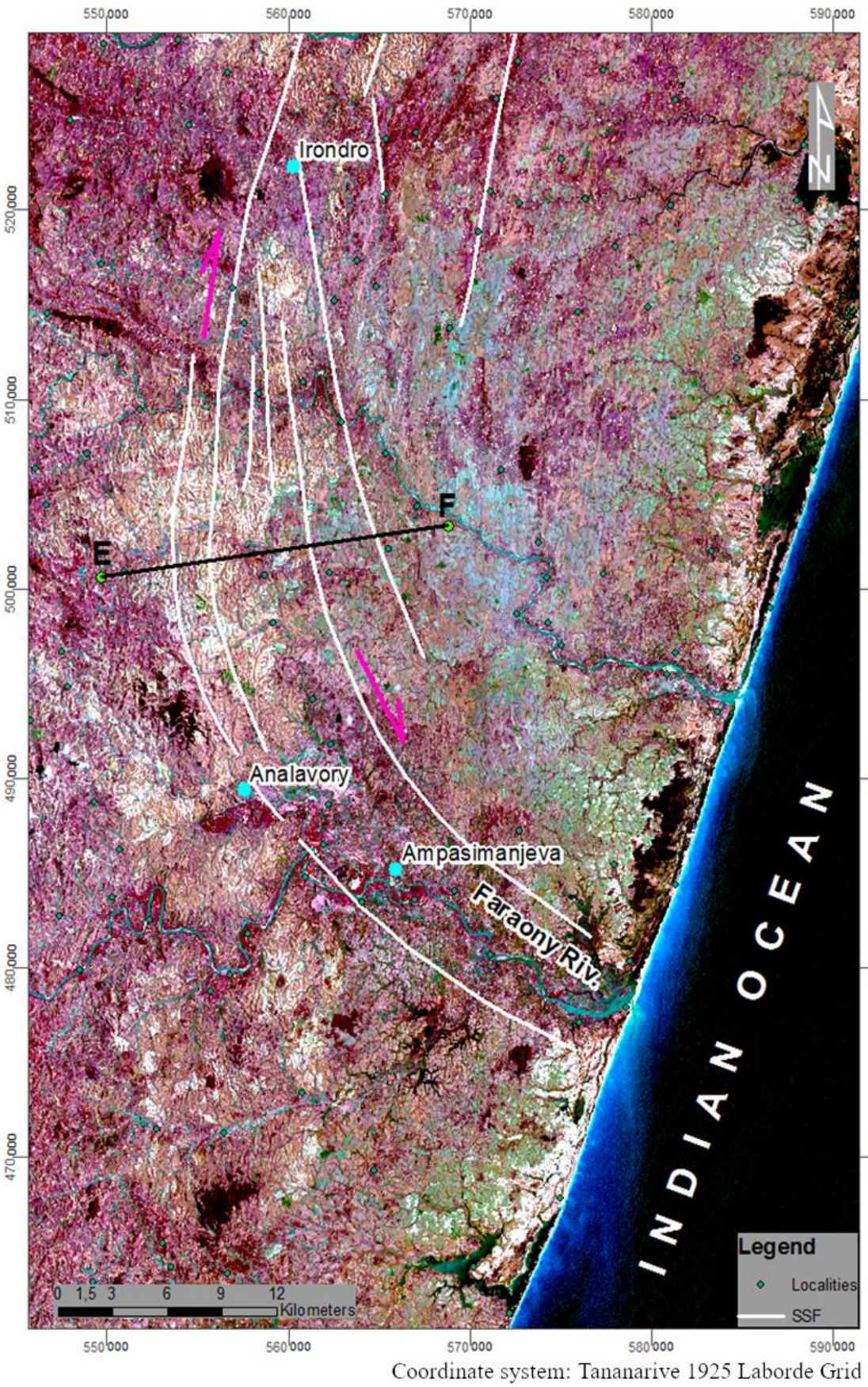

Figure 9. Ampasimanjeva compressional horsetail splay on color composite Landsat 8 image RGB743. Faraony River following the horsetail splay structure before reaching the Indian Ocean.

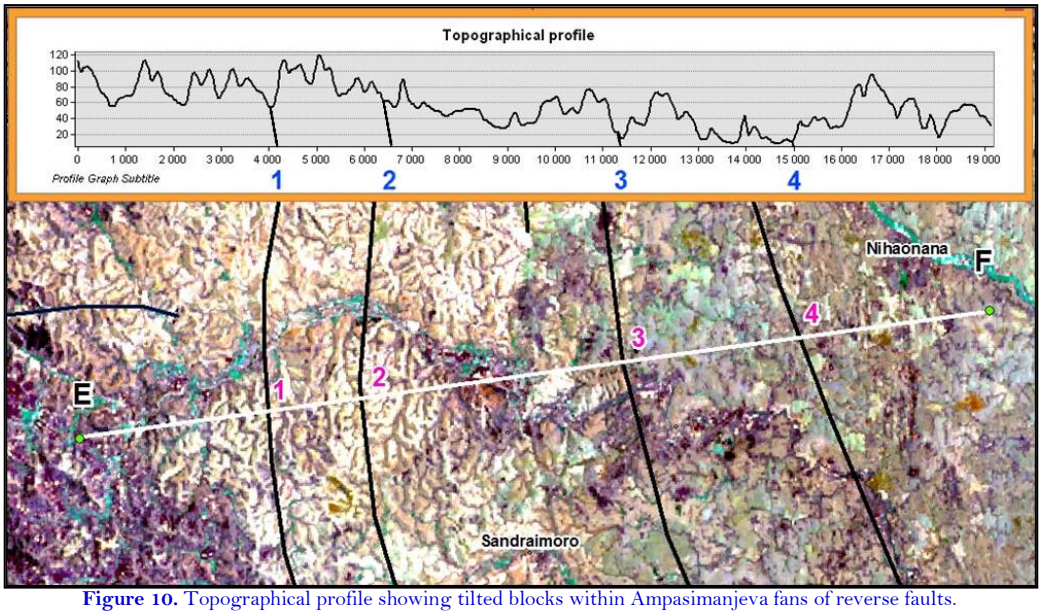

Figure 10. Topographical profile showing tilted blocks within Ampasimanjeva fans of reverse faults.

5.3.3. Push-Up

The positive flower structure unveiled around Sahamirovana village (Andriamanatsara, 2017) was confirmed by the present study. DEM analysis showed an individual massif with anomalously high topographic elevation between Vohilava and Morafeno where fault bends were observed. Left stepping of dextral SSF produces restraining bends which are sites of topographic uplifts and crustal shortening (Cunningham & Mann, 2007). The structure which I call Vohilava structure is thought to be the result of the restraining bend responsible for the thickening of the crust Figure 11.

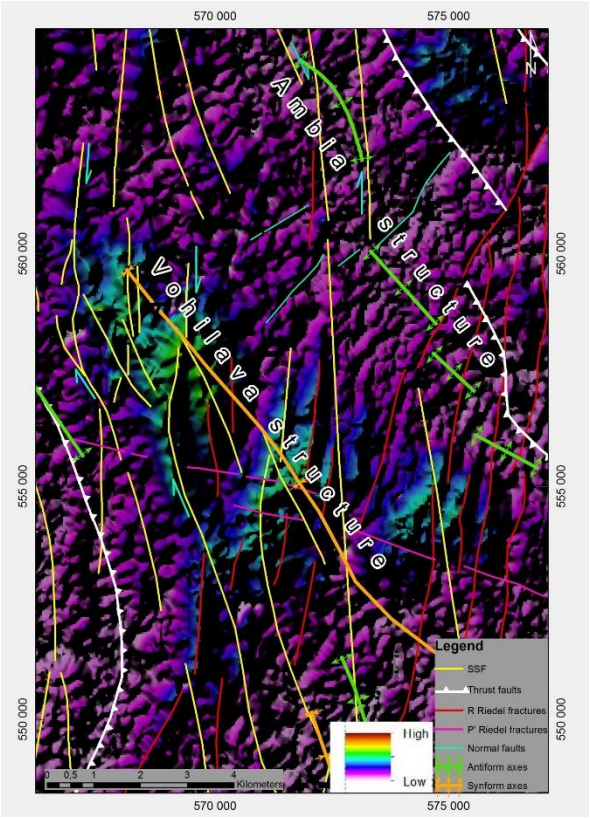

Figure 11. Ambia structure parallel to Vohilava push-up structure on ASTGTM scale 1/60 000. Fragmented, split and deformed antiform due to SSF and associated faults.

5.3.4. Associated Folds

Analysis revealed that SSF controlled the spatial distribution of Vohilava-Nosivolo and Maha groups Figure 12. The most important occurrence is in the Vohilava area where these formations were deposited within a 400 km² NW-SE basin which I call Vohilava Archean basin (VAB) extending from Marokarima in the south to Andranotonga in the north Figure 6.

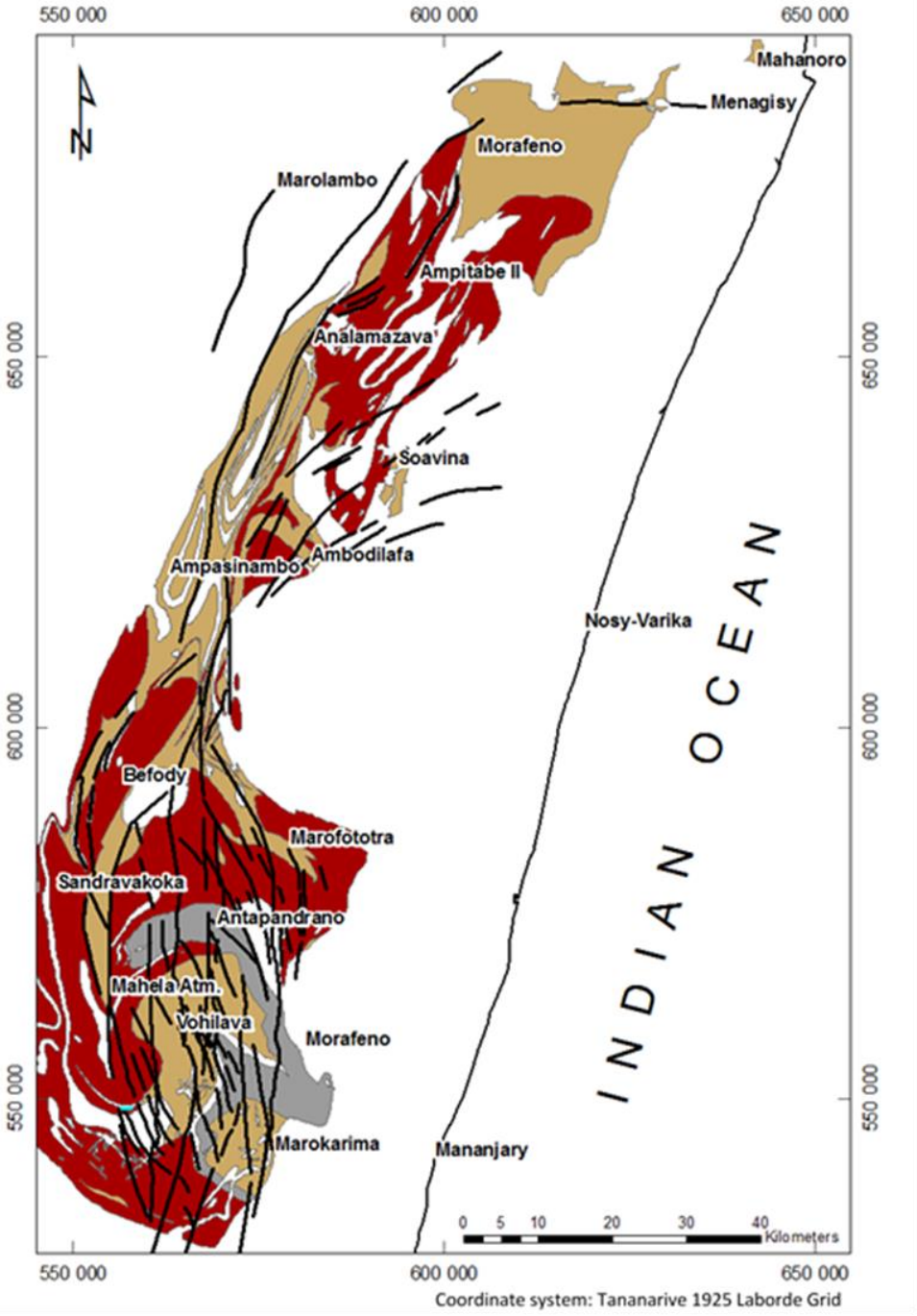

Figure 12. Map modified from Tucker et al. (2012) showing SSF control on Vohilava-Nosivolo and Maha groups spatial distribution and association of their protolith host structures (basin, graben, depression) with the SSF activities.

The basin axis is in line with the fold orientation associated with the dextral SSF. In Marofototra area, Vohilava sub-group protolith deposition happened within a 20km elongated NW-SE depression parallel to the VAB. The folding affected not only the Vohilava sub-group but also the Maha group in the VAB. Landsat OLI8 image analysis

showed that Vohilava structure which was a 10km strike synform with a N140° axis, had an antiform pair which I call Ambia structure and was located at 4km to the north Figure 11. These two structures are parallel and have almost the same length. Ambia structure is obvious as the Maha group surrounds the Vohilava sub-group from Vohilava to Antapandrano through Morafeno and Ambia. The structure is fragmented and split in four parts due to the SSF and associated faults. Resulting smaller structures are called East Manakana, West Manakana, Besaonjo and West Ambia structures. The orientation of these two structures is in accordance with the model of NS oriented dextral SSF. The analysis revealed as well another antiform with the same orientation and striking over 6km, running between Vohilava and Lambonjiro villages. Two smaller en-échelon folds parallel to the main Vohilava structure occur in the north of Sahamanara. The NW-SE orientation of these folds confirms that they were generated by the same tectonic event. Another fold oriented N170° is located at 4km distance south of Vohilava village. Its orientation is parallel to mapped thrust faults. It was probably generated by the compressive force at the origin of the thrust; two more folds occur in the south of Ambohimiarina and another one in the north of Andranotonga. These folds form a group of smaller folds parallel to thrust faults.

5.3.5. Regional Shear Zone

The AOS was affected as well by four regional N125° sinistral shear zones which I call Marovato (MaSZ), Ampitabe (ApSZ), Morafeno (MoSZ) and Ambodivato (AbSZ) shear zones Figure 6. MoSZ is the most important in terms of width which can reach 5km. MoSZ affected the SSF and was at the origin of a 3km horizontal displacement in the west of Morafeno village. Another horizontal displacement of 250m is observed at the intersection of ApSZ with the SSF at 0.5km north of Marohita village.

5.3.6. Age of Vohilava SSF

The oldest SSF footprint is the contact between Vohilava (mANBv) sub-group and Befody migmatitic othogneiss (mANBbg) from Mahela-Atsimo to Sandravakoka where a N-S oriented graben is observed Figure 13. The SSF role in the spatial distribution of Vohilava sub-group is strong evidence of the structure existence in Meso-Neoarchean. The SSF was quite active before Paleoproterozoic. Vohilava formation (nANBv) was folded in Paleoproterozoic to allow the deposition of Maha formation protolith (pPMHm) in the east of Vohilava where the Vohilava structure is. The study showed as well that R Riedel fractures trending N030° affecting the Imorona-Itsindro granite gneiss (nPIIhg) between Ambodinato and Sahamanara is evidence of its activity after Neoproterozoic Figure 6; SSF activity during Cambrian is proved by the occurrence of Riedel fractures on syeno-granite Ambalavao suite (ϵAsg) around Marohita.

N125° regional shear zones which are thought to be associated with the breakdown of Madagascar with India in Upper Cretaceous, cross-cut the SSF in different locations. These faults were at the origin of not only ductile but also brittle deformations. Footprints of the ductile deformation from MoSZ and AbSZ are visible on the eastern branch of the SSF which is curvy between Ambia and Marokarima. The master SSF underwent brittle deformation from MoSZ between Vohilava and Ambia. Some faults associated with the SSF crosscut the cretaceous volcanics near Ampasimanjeva in the south and around Ambodilafa in the north. This fact provides evidence of SSF activity after cretaceous. The SSF age is then Mesoarchean. It is younger than the formation of the Befody migmatitic orthogneiss (mANBbg) and older than the deposition of Vohilava sub-group protolith (mANBv) with a respective age 3.3-3.1Ga and 2.8-2.5Ga (Tucker et al., 2012). It remained active after cretaceous.

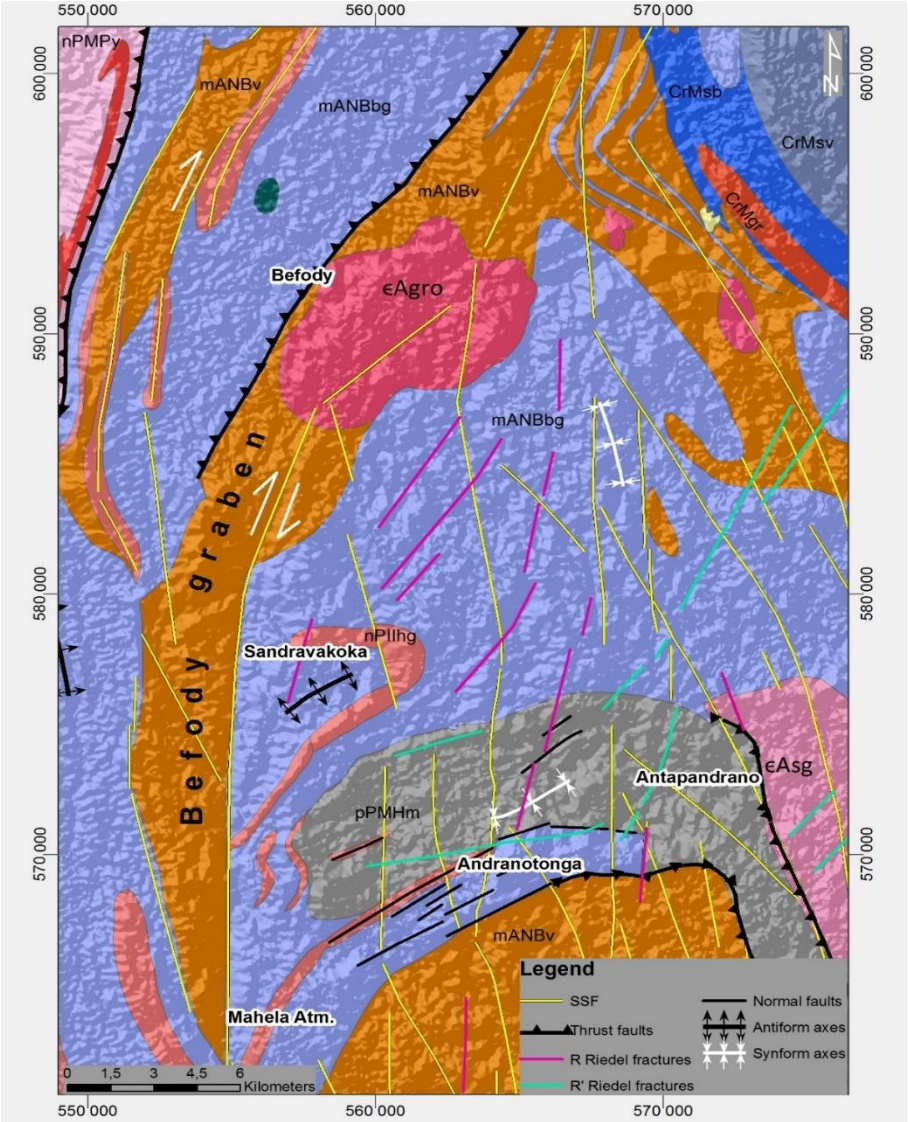

Figure 13. Geological map scale 1/150 000 displaying the tectonic contact between migmatitic orthogneiss (mANBbg) and Vohilava sub-group (mANBv) in the area located between Mahela Atsimo and Sandravakoka. Note the SSF control on Vohilava sub-group and Maha group.

6. CONCLUSION

A combination of airborne magnetometry and remote sensing has been used to regionally map the Vohilava area. In addition to the derivative-based filters THDR and AS, local phase-based filters (TDR, Theta-map, TDX, HD-TDR, TAHG, ETHDR) and signum transform have been used to detect subtle signals and separate closely spaced bodies respectively. This approach helped identify a 240km strike Mesoarchean dextral SSF striking from Mahanoro District to Manakara District. Vohilava area is now identified as a contractional duplex in a restraining bend. The SSF is also at the origin of the VAB, the APB and the Vohilava flower structure. The analysis of the Vohilava-Nosivolo and Maha groups' spatial distribution particularly within the VAB and APB led to a conclusion that the SSF development started in the south and progressively moved northward. Without regional mapping methods, it would be impossible to find structural elements that might control the gold mineralization within the Mananjary District-Madagascar. The SSF is among key elements making the area permissive for associated deposit types. New approach to exploration of associated gold deposit types is required.

Funding: This study received no specific financial support.
Competing Interests: The authors declare that they have no competing interests.
Authors' Contributions: Both authors contributed equally to the conception and design of the study.

REFERENCES

Andriamanatsara, M. F. (2017). *Study of the gold potential of the sahamirovana mananjary madagascar zone.* [Master Thesis, Université Polytechnique de Madagscar] Final Dissertation, 45-46.

Ansari, A. H., & Alamdar, K. (2011). A new edge detection method based on the analytic signal of tilt angle (ASTA) for magnetic and gravity anomalies. *Iranian Journal of Science and Technology, 82*(2), 81-88.

Arisoy, M. O., & Dikmen. (2013). Edge detection of magnetic sources using enhanced total horizontal derivative of tilt angle. *Bulletin of the Earth Sciences Application and Research Centre of Hacettepe University, Yerbilimleri, 34*(1), 73-82.

Cooper, G., & Cowan, D. (2006). Enhancing potential field data using filters based on the local phase. *Computers & Geosciences, 32*(10), 1585-1591.Available at: https://doi.org/10.1016/j.cageo.2006.02.016.

Cunningham, W. D., & Mann, P. (2007). Tectonics of strike-slip restraining and releasing bends. *Geological Society, London, Special Publications, 290*(1), 1-12.Available at: https://doi.org/10.1144/290.10.

Fairhead, J. D., Green, C. M., Verduzco, B., & Mackenzie, C. (2004). A new set of magnetic field derivatives for mapping mineral prospects. *ASEG Extended Abstracts, 2004*(1), 1-4.Available at: https://doi.org/10.1071/aseg2004ab042.

Ferreira, F. J., Souza, J., Bongiolo, B. E. S. A., & Castro, L. G. (2013). Enhancement of the total horizontal gradient of magnetic anomalies using the tilt angle. *Geophysics, 78*(3), J33-J41.Available at: https://doi.org/10.1190/geo2011-0441.1.

Ismael, M. I., Menna, H., & Bülent, T. (2019). Edge detectors as structural imaging tools using aeromagnetic data: A case study of Sohag Area. *Egypt, Geosciences, 9*(5), 211.Available at: https://doi.org/10.3390/geosciences9050211.

Marvinney, R. G., & Tucker, R. (1989). Thrust and strike-slip faults near Jackman, Maine. *Studies in Maine Geology, 1*(2), 173-185.

Miller, H. G., & Singh, V. (1994). Potential field tilt—a new concept for location of potential field sources. *Journal of Applied Geophysics, 32*(2-3), 213-217.Available at: https://doi.org/10.1016/0926-9851(94)90022-1.

Shahverdi, M., Namaki, L., Montahaei, M., Mesbahi, F., & Basavand, M. (2017). Interpretation of magnetic data based on tilt derivative methods and enhancement of total horizontal gradient, a case study: Zanjan depression. *Journal of the Earth and Space Physics, 43*, 101 -113.

Souza, J., & Ferreira, F. J. (2015). The application of the Signum transform to the interpretation of magnetic anomalies due to prismatic bodies. *ASEG Extended Abstracts, 2015*(1), 1-5.Available at: https://doi.org/10.1071/aseg2015ab190.

Sylvester, A. G., & Smith, R. R. (1976). Tectonic transpression and basement-controlled deformation in san andreas fault zone. *Salton Trough, California, The American Association of Petroleum Geologists Bulletin, 60*, 226.Available at: https://doi.org/10.1306/c1ea3a73-16c9-11d7-8645000102c1865d.

Tucker, R. D., Peters, S. G., Roig, J. Y., Théveniaut, H., & Delor, C. (2012). Explanatory note of the geological and metallological maps of the Republic of Madagascar at 1/1,000,000. *Ministry of Mines, Antanarivo, Republic of Madagascar, 36*(91), 94-109.

USGS-BGS. (2008a). Geological map of Madagascar 1:100,000 Sheet N° Q51 Ampasinambo, Mineral Resources Governance Project, Ministry of Energy and Mines of Madagascar.

USGS-BGS. (2008b). Geological map of Madagascar 1:100,000 Sheet N° R50 Marolambo, Mineral Resources Governance Project, Ministry of Energy and Mines of Madagascar.

USGS-BGS. (2008c). Geological map of Madagascar 1:100,000 Sheet N° R51 Vohitrandriana, Mineral Resources Governance Project, Ministry of Energy and Mines of Madagascar.

USGS-BGS. (2008d). Geological map of Madagascar 1:100,000 Sheet N° R52 Antsindra/Ambohinihaonana, Mineral Resources Governance Project, Ministry of Energy and Mines of Madagascar.

Williams, S. E., & Fairhead, J. D. (2006). Evaluation of normalized magnetic derivatives for structural mapping. *Society of Exploration Geophysicists*, 845-849.Available at: https://doi.org/10.1190/1.2370388.